2000

Line-shape Predictions via Bethe Ansatz for the One-dimensional Spin-1/2 Heisenberg Antiferromagnet in a Magnetic Field

Michael Karbach

Gerhard Müller
University of Rhode Island, gmuller@uri.edu

Citation/Publisher Attribution
M. Karbach and G. Müller. Lineshape predictions via Bethe ansatz for the one-dimensional spin-1/2 Heisenberg antiferromagnet in a magnetic field. Physical Review B, 62(2000), 14871-14879.
Available at: http://dx.doi.org/10.1103/PhysRevB.62.14871

Line-shape predictions via Bethe ansatz for the one-dimensional spin-$\frac{1}{2}$ Heisenberg antiferromagnet in a magnetic field

Michael Karbach[1] and Gerhard Müller[2]
[1]*Bergische Universität Wuppertal, Fachbereich Physik, D-42097 Wuppertal, Germany*
[2]*Department of Physics, University of Rhode Island, Kingston, Rhode Island 02881-0817*
(Received 10 May 2000)

The spin fluctuations parallel to the external magnetic field in the ground state of the one-dimensional (1D) $s=\frac{1}{2}$ Heisenberg antiferromagnet are dominated by a two-parameter set of collective excitations. In a cyclic chain of N sites and magnetization $0<M_z<N/2$, the ground state, which contains $2M_z$ spinons, is reconfigured as the physical vacuum for a different species of quasiparticles, identifiable in the framework of the coordinate Bethe ansatz by characteristic configurations of Bethe quantum numbers. The dynamically dominant excitations are found to be scattering states of two such quasiparticles. For $N\to\infty$, these collective excitations form a continuum in (q,ω) space with an incommensurate soft mode. Their matrix elements in the dynamic spin structure factor $S_{zz}(q,\omega)$ are calculated directly from the Bethe wave functions for finite N. The resulting line-shape predictions for $N\to\infty$ complement the exact results previously derived via algebraic analysis for the exact two-spinon part of $S_{zz}(q,\omega)$ in the zero-field limit. They are relevant for neutron-scattering experiments on quasi-1D antiferromagnetic compounds in a strong magnetic field.

I. INTRODUCTION

Advances in experimental techniques combined with improvements in sample preparation make it possible to produce data of ever increasing resolution for the quantum fluctuations and the underlying collective excitations in quasi-one-dimensional (1D) magnetic compounds. Advances in the theoretical analysis of relevant model systems combined with progress in the computational treatment of aspects that remain elusive to exact analysis make it possible to gain an ever more profound understanding of the observable collective excitations in terms of a small number of constituent quasiparticles.

There is scarcely a better case for illustrating this multitrack advancement of understanding quantum fluctuations than the 1D $s=\frac{1}{2}$ Heisenberg antiferromagnet and the growing number of materials that have been discovered to be physical realizations of this model system. The Hamiltonian for N spins $\frac{1}{2}$ arranged in a cyclic chain with isotropic exchange coupling J between nearest neighbors and a uniform magnetic field h,

$$H=\sum_{n=1}^{N}\,[J\mathbf{S}_n\cdot\mathbf{S}_{n+1}-hS_n^z], \tag{1}$$

is amenable to exact analysis via Bethe ansatz[1,2] and displays dynamical properties of intriguing complexity. The field h is a controllable continuous parameter, which leaves the eigenvectors unaltered, but changes the nature of the ground state via level crossings and thus has a strong impact on the dynamical properties, in particular at low temperatures.

At $h\geqslant h_S=2J$ the ground state of H has all spins aligned in field direction: $|F\rangle\equiv|\uparrow\uparrow\cdots\uparrow\rangle$ is the reference state of the coordinate Bethe ansatz, and all eigenstates are described as excitations of interacting magnons, a species of spin-1 quasiparticles. Hence $|F\rangle$ plays the role of the magnon vacuum. The ground state $|A\rangle$ of H at $h=0$ contains $N/2$ magnons. The Bethe ansatz enables us to reconfigure this state as the physical vacuum for a different species of quasiparticles—the spinons, which have spin $\frac{1}{2}$. The entire spectrum of the Heisenberg model (1) can also be generated as composites of interacting spinons.[3]

Both descriptions are valid throughout the spectrum, but the magnon interpretation is more useful near the magnon vacuum, and the spinon picture is more useful near the spinon vacuum. The interaction energy of magnon scattering states or spinon scattering states is of $O(N^{-1})$ as long as the number of quasiparticles in the collective excitations is of $O(1)$.[4,28] In a macroscopic system, the spectrum of such states is thus indistinguishable from the corresponding free quasiparticle states. Even under these simplifying circumstances, however, the interaction of the quasiparticles remains important in the make-up of collective wave functions, and is likely to strongly affect the transition rates and line shapes.

At intermediate values $0<h<h_S$ of the magnetic field, the number of magnons or spinons contained in the ground state of H is of $O(N)$, implying that the interaction energy for either quasiparticle species remains nonzero for $N\to\infty$ in the ground state and in all low-lying excitations. This obscures the role of individual magnons or spinons in the collective excitations and obstructs the interpretation of spectral data obtained by experimental or computational probes.

We can circumvent this problem by configuring the ground state $|G\rangle$ at $0<M_z/N<\frac{1}{2}$ as the physical vacuum for yet a different species of quasiparticles. From the new vantage point, the dynamically relevant collective excitations are then again scattering states of few quasiparticles with an interaction energy of $O(N^{-1})$, which greatly facilitates the interpretation of the spectra probed experimentally or computationally.

II. DYNAMIC STRUCTURE FACTOR

In an inelastic neutron-scattering experiment performed at low temperature, the observable scattering events predomi-

nantly involve transitions from the ground state to a subset of collective excitations filtered from the rest by selection rules and transition rates. Under idealized circumstances, the scattering cross section is proportional to the $T=0$ dynamic spin structure factor

$$S_{\mu\mu}(q,\omega)=2\pi\sum_{\lambda}\ |\langle G|S^{\mu}_{q}|\lambda\rangle|^{2}\delta(\omega-\omega_{\lambda}), \tag{2}$$

where $S^{\mu}_{q}=N^{-1/2}\Sigma_{n}e^{iqn}S^{\mu}_{n}$, $\mu=x,y,z$ is the spin fluctuation operator. In a macroscopic system, the aggregate of spectral lines in Eq. (2) pertaining to scattering events with energy transfer $\omega_{\lambda}\equiv E_{\lambda}-E_{G}$, momentum transfer $q\equiv k_{\lambda}-k_{G}$, and transition rate $|\langle G|S^{\mu}_{q}|\lambda\rangle|^{2}$ form characteristic patterns of spectral weight in (q,ω) space. The shape of the spectral weight distribution provides key information on how the dynamically relevant collective excitations are composed of quasiparticles with specific energy-momentum relations.

Experimentally it is possible, at least in principle, to separate the information contained in the dynamic structure factors of the spin components parallel and perpendicular to the field direction, i.e., the functions $S_{zz}(q,\omega)$ and $S_{xx}(q,\omega)=\frac{1}{4}[S_{+-}(q,\omega)+S_{-+}(q,\omega)]$, respectively, for the fluctuation operators S^{z}_{q} and $S^{\pm}_{q}=S^{x}_{q}\pm iS^{y}_{q}$. At $h=0$ the additional symmetry of H dictates that $S_{zz}(q,\omega)=\frac{1}{2}S_{+-}(q,\omega)=\frac{1}{2}S_{-+}(q,\omega)$.

An anchor point for the new results presented in the following is the exact two-spinon dynamic spin structure factor at $T=0$, which was determined recently via algebraic analysis and shown to contribute 73% of the total intensity in $S_{zz}(q,\omega)$ at $h=0$.[5] Given the energy-momentum relation[2]

$$\epsilon_{sp}(p)=\frac{\pi}{2}J\sin p,\quad 0\leqslant p\leqslant\pi, \tag{3}$$

of the spinon quasiparticle, the two-spinon states with wave numbers $q=p_{1}+p_{2}$ and energy $\omega=\epsilon_{sp}(p_{1})+\epsilon_{sp}(p_{2})$ form a continuum confined by the boundaries[6,7]

$$\epsilon_{L}(q)=\frac{\pi}{2}J|\sin q|,\quad \epsilon_{U}(q)=\pi J\left|\sin\frac{q}{2}\right|, \tag{4}$$

as illustrated in Fig. 1 (inset). The main plot shows the exact two-spinon line shapes of $S_{zz}(q,\omega)$ at $q=\pi/2,3\pi/4,\pi$. The most detailed experimental data available for testing these results pertain to $KCuF_{3}$.[8]

We shall see that the magnetic field causes dramatic changes in both the spectrum and the line shapes. At the root of these changes is a change in the nature of the relevant quasiparticles. Two compounds suitable for studying magnetic-field effects on spectrum and line shapes are $Cu(C_{6}D_{5}COO)_{2}\cdot 3D_{2}O$ and $Cu(C_{4}H_{4}N_{2})(NO_{3})_{2}$.[9,10]

III. BETHE ANSATZ EQUATIONS

The Bethe ansatz[1] is an exact method for the calculation of eigenvectors of integrable quantum many-body systems. The Bethe wave function of any eigenstate of Eq. (1) in the invariant subspace with $r=N/2-M_{z}$ reversed spins relative to the magnon vacuum

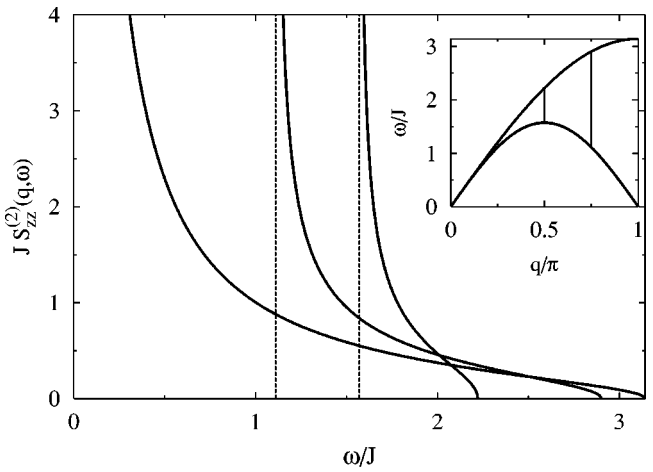

FIG. 1. Exact two-spinon line shapes at $q=\pi/2,3\pi/4,\pi$ of $S_{zz}(q,\omega)$ at $T=0$ for Hamiltonian (1) at $h=0$ as determined via algebraic analysis. The inset shows the boundaries (4) of the two-spinon spectrum.

$$|\psi\rangle=\sum_{1\leqslant n_{1}<\cdots<n_{r}\leqslant N}a(n_{1},\ldots,n_{r})S^{-}_{n_{1}}\cdots S^{-}_{n_{r}}|F\rangle, \tag{5}$$

has coefficients of the form

$$a(n_{1},\ldots,n_{r})=\sum_{\mathcal{P}\epsilon S_{r}}\exp\left(i\sum_{j=1}^{r}k_{\mathcal{P}_{j}}n_{j}+\frac{i}{2}\sum_{i<j}^{r}\theta_{\mathcal{P}_{i}\mathcal{P}_{j}}\right) \tag{6}$$

determined by r magnon momenta k_{i} and one phase angle $\theta_{ij}=-\theta_{ji}$ for each magnon pair. The sum $\mathcal{P}\in S_{r}$ is over the permutations of the labels $\{1,2,\ldots,r\}$.

The consistency requirements for the coefficients $a(n_{1},\ldots,n_{r})$ inferred from the eigenvalue equation $H|\psi\rangle=E|\psi\rangle$ and the requirements imposed by translational invariance lead to a set of coupled nonlinear equations for the k_{i} and θ_{ij}. A computationally convenient rendition of the Bethe ansatz equations has the form

$$N\phi(z_{i})=2\pi I_{i}+\sum_{j\neq i}\phi[(z_{i}-z_{j})/2],\quad i=1,\ldots,r, \tag{7}$$

where $\phi(z)\equiv 2\arctan z$, $k_{i}=\pi-\phi(z_{i})$ and $\theta_{ij}=\pi\,\mathrm{sgn}[\mathrm{Re}(z_{i}-z_{j})]-\phi[(z_{i}-z_{j})/2]$. Every real solution of Eq. (7) is specified by a set of Bethe quantum numbers $I_{1}<I_{2}<\ldots<I_{r}$, which assume integer values for odd r and half-integer values for even r. The energy and wave number of the eigenvector thus determined are

$$\frac{E-E_{F}}{J}=-\sum_{i=i}^{r}\frac{2}{1+z_{i}^{2}},\quad k=\pi r-\frac{2\pi}{N}\sum_{i=1}^{r}I_{i}, \tag{8}$$

where $E_{F}=JN/4$ is the energy of the magnon vacuum.

We consider the class K_{r} of eigenstates whose Bethe quantum numbers comprise, for $0\leqslant r\leqslant N/2$ and $0\leqslant m\leqslant N/2-r$, all configurations

$$-\frac{r}{2}+\frac{1}{2}-m\leqslant I_{1}<I_{2}<\cdots<I_{r}\leqslant\frac{r}{2}-\frac{1}{2}+m. \tag{9}$$

Here we employ the solutions $\{z_{i}\}$ of the Bethe ansatz equations not only to generate spectral data via Eq. (8),

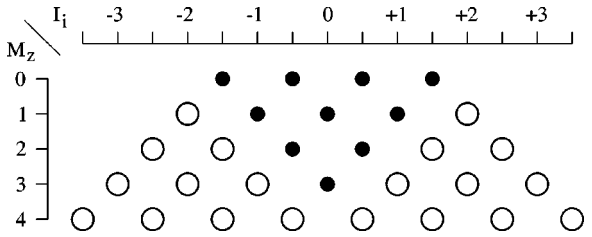

FIG. 2. Physical vacuum $|G\rangle$ for a chain of $N=8$ spins at magnetization $M_z=0,1,...,4$. The values of the Bethe quantum numbers I_i are given by the positions of the magnons (●). The spinons (○) correspond to vacancies in the I_i configurations.

which is standard practice, but also to evaluate transition rates $|\langle G|S_q^\mu|\lambda\rangle|^2$ for the dynamic structure factor (2) directly from the normalized Bethe wave functions $|\lambda\rangle \equiv|\psi\rangle/\|\psi\|$. The computational aspects of this method are discussed elsewhere.[11]

IV. PHYSICAL VACUUM AND QUASIPARTICLES

The ground-state wave function $|G\rangle$ at $0\leqslant M_z\leqslant N/2$ is specified by the set of $r=N/2-M_z$ Bethe quantum numbers[12]

$$\{I_i\}_G=\left\{-\frac{N}{4}+\frac{M_z}{2}+\frac{1}{2},\ldots,\frac{N}{4}-\frac{M_z}{2}-\frac{1}{2}\right\}. \qquad (10)$$

As the magnetic field increases from $h=0$ to $h_S=2J$, the magnetization M_z increases in units of one from zero to $N/2$. A sequence of level crossings produces a magnetization curve (M_z/N versus h) in the form of a staircase with $N/2$ steps of height $1/N$, which converges toward a smooth line as $N\to\infty$.[13–15]

Depending on the reference state used for the characterization of the ground state $|G\rangle$, it can be regarded as a scattering state of $N/2-M_z$ magnons excited from the magnon vacuum $|F\rangle$ or as a scattering state of $2M_z$ spinons excited from the spinon vacuum $|A\rangle$. To illustrate the distinct roles played by the two species of quasiparticles in the class-K_r states, we show in Fig. 2 the configuration of Bethe quantum numbers for $|G\rangle$ in a system with $N=8$ and all values of M_z realized between $h=0$ and $h=h_S$. The positions of the magnons (●) are determined by the set (10) of I_i's and the positions of the spinons (○) by the vacancies across the full range of the I_i's allowed by Eq. (9) for class K_r states.

Henceforth we treat $|G\rangle$ as the new physical vacuum. At $h=0$ (top row in Fig. 2) it coincides with the spinon vacuum, a state with $N/2$ magnons. At $h=h_S$ (bottom row) it coincides with the magnon vacuum, a state containing N spinons. All states within class K_r are generated from $|G\rangle$ by rearranging the magnons or (equivalently) the spinons into all allowed configurations.

For $r=N/2$ (top row) and $r=0$ (bottom row) the state shown is the only possible configuration within class K_r. In the fourth row, the lone magnon can be moved across the array of spinons, generating a branch (one-parameter set) of one-magnon excitations for $N\to\infty$. In the second row, the two spinons can be moved independently across the array of magnons, generating a continuum (two-parameter set) of two-spinon excitations for $N\to\infty$ with boundaries (4) as shown in Fig. 1. The center row in Fig. 2 pertains to the field at half the saturation magnetization ($M_z=r=N/4$), the case we shall investigate extensively for various system sizes. Here $|G\rangle$ contains twice as many spinons as it contains magnons.

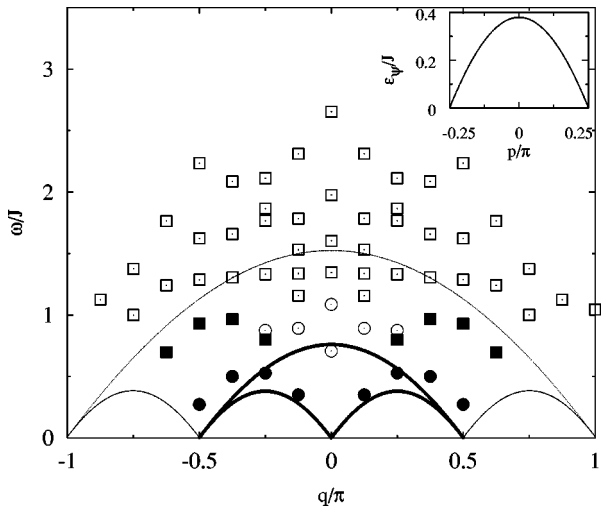

FIG. 3. Spectrum of two-psinon excitations (circles) and four-psinon excitations (squares) for $M_z=N/4$ and $N=16$. The states marked by full symbols are dynamically dominant in $S_{zz}(q,\omega)$. The spectral ranges of the two-psinon states (thick lines) and four-psinon states (thin lines) for $N\to\infty$ are inferred from data for $N=2048$. The inset shows the psinon energy momentum relation $\epsilon_\psi(p)$.

The integer m with range $0<m\leqslant M_z$ used in (9) is a convenient quantum number for the subdivision of the classes K_r. Every state of K_r at fixed m can then be regarded as a scattering state of m pairs of spinonlike quasiparticles. To distinguish them from the spinons, we name the new quasiparticles ''psinons.''

The ground state $|G\rangle$, the only state with $m=0$, is the psinon vacuum. Here the magnons form a single array flanked by two arrays of spinons (see Fig. 2). Relaxing the constraint in (9) from $m=0$ to $m=1$ yields a two-parameter set of states—the two-psinon excitations. Here the array of magnons breaks into three clusters separated by the two innermost spinons, which now assume the role of psinons. The remaining $2M_z-2$ spinons stay sidelined. In the four-psinon states ($m=2$), two additional spinons have been mobilized into psinons. By this prescription, we can systematically generate sets of $2m$-psinon excitations for $0\leqslant m\leqslant M_z$.

To illustrate the quasiparticle role of the psinons in the class-K_r collective states we have plotted in Fig. 3 energy versus wave number of all two-psinon states (circles) and four-psinon states (squares) at $M_z=N/4$ for $N=16$. Also shown are the spectral boundaries of two-psinon and four-psinon states for $N\to\infty$ as inferred from solutions of Eq. (7) for $N=2048$. The two-psinon continuum, outlined by thick lines, is confined to the interval $|q|\leqslant q_s$, where

$$q_s\equiv\pi(1-2M_z/N) \qquad (11)$$

denotes the wave number of an incommensurate soft mode. The lower four-psinon spectral boundary is the same as the two-psinon lower boundary but extended periodically over

the entire Brillouin zone. The upper four-psinon boundary is related to the upper two-psinon boundary by a scale transformation $(q \to 2q, \omega \to 2\omega)$.

The relationship between the ranges in (q,ω)-space of the two-psinon states and the four-psinon states does indeed reflect that fact that they are scattering states of two or four quasiparticles, respectively, of the same species. Similar to the spinon, the psinon is not observable in isolation via neutron scattering, but its energy momentum relation $\epsilon_\psi(p)$, $-\pi/4 \leqslant p \leqslant \pi/4$, can be inferred from the data of Fig. 3 (see inset).

If there were no psinon interaction, the wave number and energy of a $2m$-psinon state would be $q=\Sigma_{i=1}^{2m} p_i$, $\omega = \Sigma_{i=1}^{2m} \epsilon_\psi(p_i)$. The $N=16$ data make it quite clear that the finite-size energy correction caused by the psinon interaction is stronger in the four-psinon states than in the two-psinon states. In both sets of collective states, the interaction energy goes to zero as the scattering events become less and less frequent in a chain of increasing length. However, it takes longer chains for finite-N four-psinon data to reach comparable convergence toward the spectral boundaries predicted for $N \to \infty$, because for fixed N, the scattering events between psinons are more numerous in a typical four-psinon state than in a typical two-psinon state.

If instead of the psinon vacuum we had used the spinon vacuum as the reference state at $M_z = N/4$, then both the two-psinon states and the four-psinon states would have to be described as scattering states of $N/2$ spinons. Although we know the energy-momentum relation of a spinon, Eq. (3), it is of little use to determine the spectral threshold in Fig. 3. Since the two-psinon and four-psinon states maintain a finite density of spinons in the limit $N \to \infty$, the spinon interaction energy remains significant. This problem does not arise at $M_z = 0$. In the two-spinon scattering states depicted in Fig. 1, the spinon interaction energy vanishes for $N \to \infty$ just as the psinon interaction energy does in the two-psinon and four-psinon scattering states depicted in Fig. 3.[16,29]

V. DYNAMICALLY RELEVANT EXCITATIONS

At $M_z = 0$ the spectral weight in the dynamic spin structure factor $S_{zz}(q,\omega)$ is dominated by the two-spinon excitations.[5] Our task here is to determine how the spectral weight of $S_{zz}(q,\omega)$ at $M_z \neq 0$ is distributed among the $2m$-psinon excitations. In investigating this question, we follow the strategy of an older study[17] but with vastly improved conceptual and numerical tools.

We begin by exploring, in a chain of $N=16$ spins at $M_z/N = \frac{1}{4}$, the transition rates between the ground state $|G\rangle$ and all $2m$-psinon excitations for $m=0,1,2,3,4$. The Bethe quantum numbers of the states with $m=0,1$ are shown in Fig. 4. The first row represents the psinon vacuum with its four magnons sandwiched by two sets of four spinons. The two innermost spinons (marked gray) become psinons when at least one of them is moved to another position. In the rows underneath, the psinons are moved systematically across the array of magnons while the remaining spinons stay frozen in place. These eight configurations describe all two-psinon states with $q \geqslant 0$.

The wave numbers, energies, and transition rates of the states shown in Fig. 4 are listed in Table I. Remarkably,

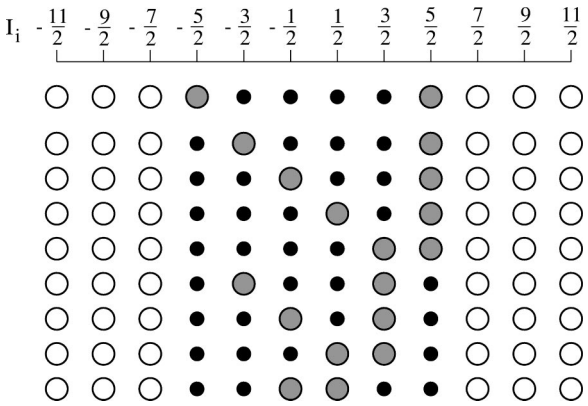

FIG. 4. Psinon vacuum $|G\rangle$ for $N=16$, $M_z=4$ and two-psinon states with $q \geqslant 0$. The I_i values are marked by the positions of the magnons (small circles). The spinons (large circles) mark I_i vacancies. A subset of the spinons are called psinons (gray circles).

almost the entire two-psinon spectral weight is concentrated in the lowest excitation for any given q. The dynamically dominant two-psinon states are marked by solid circles in Fig. 3. In a macroscopic system, they form the lower boundary of the two-psinon continuum.

Next we calculate the transition rates $|\langle G|S_q^z|\lambda\rangle|^2$ for the complete set of four-psinon states. Interestingly, we observe that most of the four-psinon spectral weight is again carried by a single branch of excitations. The dynamically dominant four-psinon states for $N=16$ are shown as full squares in Fig. 3. For large N they form a branch adjacent to the two-psinon spectral threshold.

An investigation of the remaining $2m$-psinon states shows that there exists one dynamically dominant branch of $2m$-psinon excitations for $0 < m \leqslant M_z$. The configurations of Bethe quantum numbers pertaining to the four branches for $N=16$, each consisting of $N/2 - M_z = 4$ states (at $q>0$), are shown in Fig. 5. The energies, wave numbers, and transition rates of these excitations are listed in Table II. All other $2m$-psinon excitations have transition rates that are smaller by at least two orders of magnitude at $q < \pi/2$, and still by more than one order of magnitude at $q \geqslant \pi/2$.

Inspection of Fig. 5 reveals an interesting pattern, indicative of the composition of the dynamically relevant collective excitations. They form a two-parameter set. The two parameters are highlighted by gray circles. Hitherto we have

TABLE I. Ground state $|G\rangle$ and two-psinon excitations for $N=16$, $M_z=4$, and wave numbers $q \equiv k - k_G \geqslant 0$ (in units of $2\pi/N$). The ground state has $k_G=0$ and $E_G = -11.5121346862$.

$2I_i$	$k-k_G$	$E-E_G$	$\lvert\langle G\rvert S_q^z\lvert\lambda\rangle\rvert^2$
−3−1+1+3	0	0.0000000000	1.0000000000
−5−1+1+3	1	0.3504534152	0.0484825989
−5−3+1+3	2	0.5271937189	0.0587154211
−5−3−1+3	3	0.5002699273	0.0773592284
−5−3−1+1	4	0.2722787522	0.1257902349
−5−1+1+5	0	0.7060324808	0.0000000000
−5−3+1+5	1	0.8908215652	0.0000064288
−5−3−1+5	2	0.8738923064	0.0000312622
−5−3+3+5	0	1.0855897189	0.0000000000

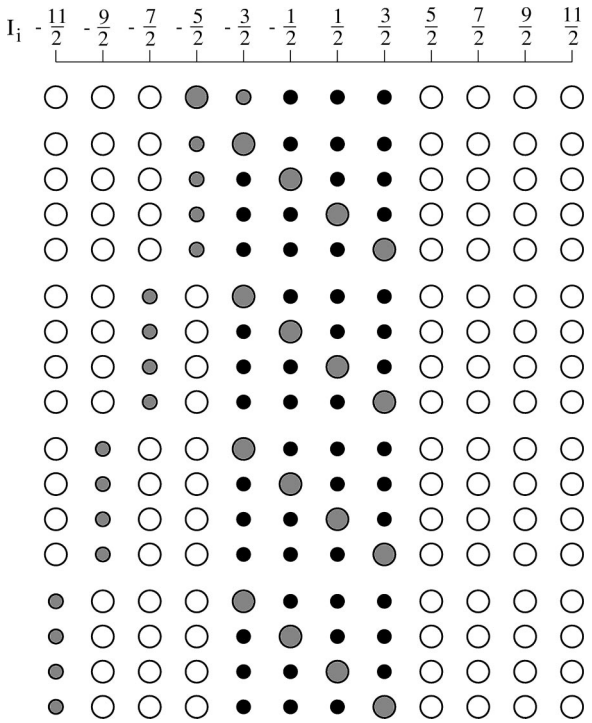

FIG. 5. Psinon vacuum $|G\rangle$ for $N=16$, $M_z=4$ and set of $\psi\psi^*$ states with $0\leqslant q\leqslant\pi$. The I_i are given by the positions of the magnons (small circles) in each row. The spinons (large circles) correspond to I_i vacancies. The psinon (ψ) and the antipsinon (ψ^*) are marked by a large and a small gray circle, respectively.

interpreted each group of four configurations as a branch of $2m$-psinon excitations, which are seemingly arbitrary one-parameter subsets taken from $2m$-parameter sets of states. In a macroscopic system, all but the lowest such branches contain a macroscopic number of psinons. Hence the range of

TABLE II. Ground state and dynamically dominant excitations for ($N=16$, $r=4$) among $2m$-psinon states ($m=0,1,...,4$). The latter form the $\psi\psi^*$ continuum in the limit $N\rightarrow\infty$. The wave numbers $q\equiv k-k_G\geqslant 0$ are in units of $2\pi/N$.

$2I_i$	$2m$	q	$E-E_G$	$\lvert\langle G\lvert S^z_q\rvert\lambda\rangle\rvert^2$
$-3-1+1+3$	0	0	0.0000000000	1.0000000000
$-5-1+1+3$	2	1	0.3504534152	0.0484825989
$-5-3+1+3$	2	2	0.5271937189	0.0587154211
$-5-3-1+3$	2	3	0.5002699273	0.0773592284
$-5-3-1+1$	2	4	0.2722787522	0.1257902349
$-7-1+1+3$	4	2	0.7981588810	0.0426892576
$-7-3+1+3$	4	3	0.9653287066	0.0552255878
$-7-3-1+3$	4	4	0.9301340415	0.0743667351
$-7-3-1+1$	4	5	0.6966798553	0.1253357676
$-9-1+1+3$	6	3	1.2708459328	0.0345439774
$-9-3+1+3$	6	4	1.4285177129	0.0516860817
$-9-3-1+3$	6	5	1.3858078992	0.0753564030
$-9-3-1+1$	6	6	1.1488426600	0.1406415212
$-11-1+1+3$	8	4	1.6819046570	0.0235815843
$-11-3+1+3$	8	5	1.8257803105	0.0443726010
$-11-3-1+3$	8	6	1.7724601200	0.0744641955
$-11-3-1+1$	8	7	1.5309413164	0.1686893882

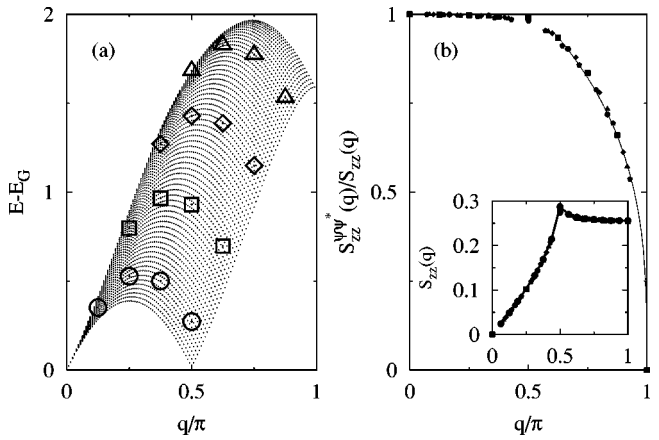

FIG. 6. (a) $\psi\psi^*$ excitations at $M_z/N=\frac{1}{4}$ for $N=16$ (circles, squares, diamonds, triangles for $m=1,2,3,4$, respectively) and $N=256$ (dots). (b) Integrated intensity $S_{zz}(q)$ (inset) and relative $\psi\psi^*$ contribution (main plot) for $N=12,16,20,24,28,32$. The lines connect the $N=32$ data points.

the dynamically relevant excitations in (q,ω) space cannot be inferred from the psinon energy-momentum relation alone as was possible for the two-psinon and four-psinon continua, because the psinon interaction energy will remain non-negligible in most of these states for $N\rightarrow\infty$, just as the spinon interaction energy was non-negligible in the two-psinon and four-psinon scattering states at $M_z\neq 0$.

A more natural interpretation of the pattern on display in Fig. 5 identifies one of the two parameters as a psinon (large gray circle) as before and the other parameter as a new quasiparticle (small gray circle). The latter is represented by a hole in what was one of two spinon arrays in the psinon vacuum. Instead of focusing on the cascade of psinons (mobile spinons) which this hole has knocked out of the vacuum, we focus on the hole itself, which has properties commonly attributed to antiparticles. The psinon (ψ) and the antipsinon (ψ^*) exist in disjunct parts of the psinon vacuum, namely in the magnon and spinon arrays, respectively. When they meet at the border of the two arrays, they undergo a mutual annihilation, represented by the step from the second row to the top row in Fig. 5.

We could have interpreted the small gray circle as a magnon (spin-one quasiparticle), but when we do that we must take into account that it then coexists in the magnon vacuum with a macroscopic number of fellow magnons (small black circles). From this perspective, the collective excitation must be viewed as containing a finite density of magnons (for $N\rightarrow\infty$), in which the magnon interaction remains energetically significant for scattering states. The nonzero interaction energy obscures the role of individual magnons.

On the other hand, when the small gray circle is interpreted as an antipsinon, then it lives in the psinon vacuum, i.e., almost in isolation. The only other particle present is a psinon (large gray circle). In a macroscopic system, the interaction energy in a psinon-antipsinon ($\psi\psi^*$) scattering state becomes negligible. Therefore, the identity of both quasiparticles is easily recognizable in the spectrum.

The energies versus the wave numbers of the 16 $\psi\psi^*$ states listed in Table II are shown in Fig. 6(a) as large symbols. The four branches from bottom to top pertain to m

$=1,...,4$. Also shown in the same plot are the $\psi\psi^*$ states for $N=256$. The lower boundary of the $\psi\psi^*$ continuum emerging in the limit $N\to\infty$ touches down to zero frequency at $q=0$ and $q=q_s=\pi/2$. Between q_s and π, it rises monotonically and reaches the value $E-E_G=h$. A direct observation of the incommensurate soft mode at q_s was made in a neutron-scattering experiment on $Cu(C_6D_5COO)_2\cdot 3D_2O$ (copper benzoate).[9]

Figure 6(b) shows the relative integrated intensity of the $\psi\psi^*$ excitations for various N at fixed $M_z/N=\frac{1}{4}$. At $q\lesssim q_s=\pi/2$, virtually all spectral weight of $S_{zz}(q,\omega)$ originates from $\psi\psi^*$ fluctuations. An extrapolation of the data points at $q=\pi/2$ suggests that the relative $\psi\psi^*$ spectral weight is in excess of 93%.

At $q\gtrsim q_s$ the $\psi\psi^*$ contribution to the integrated intensity decreases monotonically but stays dominant over more than half the distance to the zone boundary. The width of the $\psi\psi^*$ continuum vanishes linearly on approach of $q=\pi$, and the relative spectral weight more slowly: $S_{zz}(q)\sim(\pi-q)^\gamma$, $\gamma\simeq 0.3$. This enhances the observability of the $\psi\psi^*$ excitations in the narrow energy range near the Brillouin zone in spite of the low absolute intensity. Finite-N data for the integrated intensity $S_{zz}(q)$ are shown in the inset to Fig. 6(b). This function is peaked at $q=q_s$, where the $\psi\psi^*$ spectral weight is overwhelmingly predominant.

When we lower M_z, the soft mode at q_s moves to the right, the number of $2m$-psinon branches that contribute to the $\psi\psi^*$ continuum shrinks but each branch gains additional states. At $M_z=1$ we are left with one two-psinon branch extending over the interior of the entire Brillouin zone. This branch is equal to the lowest branch of two-spinon states with dispersion $\epsilon_L(q)$, Eq. (4). However, even for this case the psinon vacuum is different from the spinon vacuum. The former is the lowest-energy two-spinon state (with $M_z=1$), whereas the latter is a state with $M_z=0$. The wave number of the two vacua differ by π. At $M_z=0$ the $\psi\psi^*$ excitations disappear altogether. The limit $h\to 0$ of the infinite chain is very subtle and will be discussed elsewhere.[18]

When we increase M_z toward the saturation value, the soft mode moves to the left, and the number of $2m$-psinon branches increases, but each branch becomes shorter. At $M_z=N/2-1$, the two-parameter set collapses into a one-parameter set consisting of one $2m$-psinon state each for $m=1,2,...,N/2-1$. These states are more naturally interpreted as a branch of one-magnon excitations with dispersion $\epsilon_1(q)=J(1-\cos q)$. Their relative spectral weight in $S_{zz}(q,\omega)$ is now 100%, but the absolute intensity for $q\neq 0$ is only of $O(N^{-1})$.

To further illustrate the roles of the psinon and the antipsinon as the relevant quasiparticles in the collective excitations dominating the spectral weight in $S_{zz}(q,\omega)$, we compare in Fig. 7 the energies between the $\psi\psi^*$ scattering states for $N=64$ and the corresponding (fictitious) free $\psi\psi^*$ superpositions. The vertical displacement of any ($\bigcirc$) from the associated ($+$) reflects the interaction energy between the two quasiparticles. This energy approaches zero for all states of this class as $N\to\infty$.

The energy-momentum relations of the two quasiparticles can be accurately inferred from $N=2048$ data for the spectral thresholds of the $\psi\psi^*$ states as illustrated in the inset to

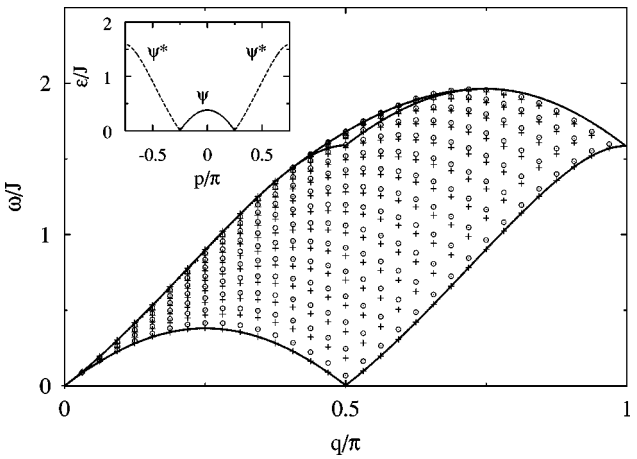

FIG. 7. Energy versus wave number of all $\psi\psi^*$ scattering states at $q\geq 0$ for $N=64(\bigcirc)$ in comparison with the corresponding free $\psi\psi^*$ states ($+$). The inset shows the energy-momentum relations of the psinon ($|p|\leq\pi/4$) and the antipsinon ($\pi/4\leq|p|\leq 3\pi/4$) as inferred from from $\psi\psi^*$ data for $N=2048$.

Fig. 7. The psinon dispersion $\epsilon_\psi(p)$ is confined to the interval at $|p|\leq\pi/4$ (solid line) and the antipsinon dispersion $\epsilon_{\psi^*}(p)$ to $\pi/4\leq|p|\leq 3\pi/4$ (dashed line). The different ranges of momentum which the two quasiparticles are allowed to have correspond to the different regions in Fig. 5 across which the circles pertaining to them can be varied.

The lower boundary of the $\psi\psi^*$ continuum is defined by collective states in which one of the two particles has zero energy: the psinon for $|q|\leq\pi/2$ and the antipsinon for $\pi/2\leq|q|\leq\pi$. The upper boundary consists of three distinct segments.

For $0\leq q\lesssim 0.3935$ the highest-energy $\psi\psi^*$ state is made up of a zero-energy psinon with momentum $p_\psi=-\pi/4$ and an antipsinon with momentum $p_{\psi^*}=\pi/4+q$. Here the shape of the continuum boundary is that of the psinon dispersion. Likewise, for $3\pi/4\leq q\leq\pi$, the states along the upper continuum boundary are made up of a maximum-energy antipsinon (with momentum $p_{\psi^*}=3\pi/4$ and a psinon with momentum $p_\psi=-3\pi/4+q$. Here the shape of the continuum boundary is that of the psinon dispersion.

When these two delimiting curves are extended into the middle segment, $0.3935\lesssim q\leq 3\pi/4$, they join in a cusp singularity at $q=\pi/2$. Here the highest $\psi\psi^*$ state does not involve any zero-energy quasiparticles. The maximum of $\epsilon_\psi(p_\psi)+\epsilon_{\psi^*}(p_{\psi^*})$ subject to the constraint $p_\psi+p_{\psi^*}=q$ does not occur at the end point of any quasiparticle dispersion curve. Consequently, the $\psi\psi^*$ continuum is partially folded about the upper continuum boundary along the middle segment.

VI. LINE SHAPES

To calculate the lineshapes relevant for fixed-q scans in an inelastic neutron-scattering experiment from the spectrum and matrix elements obtained via Bethe ansatz, we exploit key properties of transition rates and densities of states of sets of excitations that form two-parameter continua in (q,ω) space for $N\to\infty$. The $\psi\psi^*$ transition rates (scaled by N) form a continuous function $M_{zz}^{\psi\psi^*}(q,\omega)$ for $N\to\infty$.

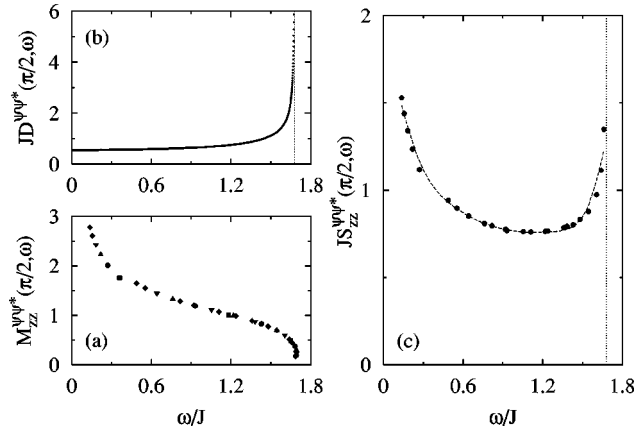

FIG. 8. (a) Density of $\psi\psi^*$ states at $q=\pi/2$ evaluated via Eq. (12) from Bethe ansatz data for $N=2048$. (b) Transition rates (13) between the psinon vacuum and the $\psi\psi^*$ states at $q=\pi/2$ for $N=12,16,20,24,28,32$. (c) Line shape at $q=\pi/2$ of the $\psi\psi^*$ contribution to $S_{zz}(q,\omega)$. All results are for $M_z=N/4$.

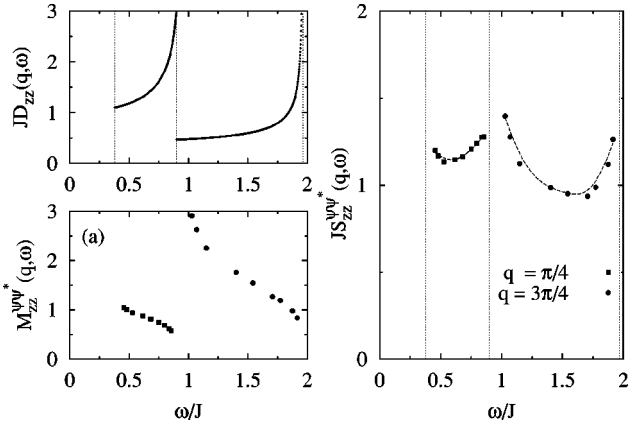

FIG. 9. (a) Density of $\psi\psi^*$ states at $q=\pi/4,3\pi/4$ evaluated via Eq. (12) from Bethe ansatz data for $N=2048$. (b) Transition rates (13) between the psinon vacuum and the $\psi\psi^*$ states at $q=\pi/4,3\pi/4$ for $N=16,24,32$. (c) Line shape at $q=\pi/4,3\pi/4$ of the $\psi\psi^*$ contribution to $S_{zz}(q,\omega)$. All results are for $M_z=N/4$.

The $\psi\psi^*$ density of states (scaled by N^{-1}) becomes a continuous function $D^{\psi\psi^*}(q,\omega)$ for $N\to\infty$. The $\psi\psi^*$ spectral-weight distribution is then the product $S_{zz}^{\psi\psi^*}(q,\omega)=D^{\psi\psi^*}(q,\omega)M_{zz}^{\psi\psi^*}(q,\omega)$.[19,30] In the following, we consider three wave numbers at $M_z=N/4$.

At $q=\pi/2$, the $\psi\psi^*$ continuum is gapless and the relative $\psi\psi^*$ spectral weight in $S_{zz}(q,\omega)$ has a maximum. The scaled density of $\psi\psi^*$ states is generated from $N=2048$ data of the set of points

$$D^{\psi\psi^*}(q,\omega_{\nu^*})\equiv\frac{2\pi/N}{\omega_{\nu^*+1}-\omega_{\nu^*}},\tag{12}$$

where $\nu^*=m$ marks the antipsinon quantum number in the $\psi\psi^*$ continuum and picks the dynamically relevant branch from the set of $2m$-psinon states. The psinon quantum number ν is adjusted to keep the wave number q of the $\psi\psi^*$ state fixed. This choice of labels produces an ordered sequence of levels. Starting at $\omega=0$, the graph of $D^{\psi\psi^*}(\pi/2,\omega_{\nu^*})$ rises from a nonzero value very slowly up to near the upper band edge, where it bends into a square-root divergence as shown in Fig. 8(a). The divergence is produced by a maximum of the sequence ω_{ν^*} at the fold of the $\psi\psi^*$ continuum.[20]

In Fig. 8(b) we show finite-N data at $q=\pi/2$ for the scaled transition rates

$$M_{zz}^{\psi\psi^*}(q,\omega_{\nu^*})\equiv N|\langle G|S_q^z|\nu^*\rangle|^2.\tag{13}$$

These data compellingly suggest the existence of a smooth function $M_{zz}^{\psi\psi^*}(\pi/2,\omega)$ for the $\psi\psi^*$ transition rates in the limit $N\to\infty$, which further highlights the physical significance of the psinon and the antipsinon as relevant quasiparticles in this situation. The function $M_{zz}^{\psi\psi^*}(\pi/2,\omega)$ is monotonically decreasing with a divergence at $\omega=0$ and a cusp singularity at the upper band edge $\omega_U\simeq 1.679J$.

The product of the transition rate function and the (interpolated) density of states is shown in Fig. 8(c).[21] The curve fitted through the data points represents the $\psi\psi^*$ line shape at $q=\pi/2$ in $S_{zz}(q,\omega)$. Its most distinctive feature is the double peak due to apparent divergences at both band edges.

The divergence at $\omega=0$, which is caused by the matrix elements, is a power law, $\omega^{-\alpha}$, with an exponent that is exactly known from field theoretic studies of the Heisenberg model.[22–24] For the situation at hand, the value is $\alpha=0.4688\ldots$. The divergence at ω_U is caused by the diverging density of states but is weakened if the cusp singularity of $M_{zz}^{\psi\psi^*}(\pi/2,\omega)$ starts from zero at $\omega=\omega_U$. The expectation is a power-law singularity, $(\omega_U-\omega)^{-\beta}$ with an exponent $0\leqslant\beta\leqslant\frac{1}{2}$.

It is interesting to compare the $\psi\psi^*$ transition rate function $M_{zz}^{\psi\psi^*}(\pi/2,\omega)$ at $M_z=N/4$ inferred from the Bethe ansatz with the two-spinon transition rate function $M_{zz}^{(2)}(\pi,\omega)$ at $M_z=0$ calculated via algebraic analysis.[5] The shape of both functions is similar, but there are some differences: $M_{zz}^{(2)}(\pi,\omega)$ has a stronger power-law divergence at $\omega=0$ and it approaches zero more rapidly at the upper band edge. As a result it produces a monotonically decreasing spectral-weight distribution $S_{zz}^{(2)}(\pi,\omega)$ (see Fig. 1) notwithstanding the fact that the two-spinon density of states is also a monotonically increasing function terminating in a square-root divergence.

At $q=\pi/4$ the integrated intensity $S_{zz}(q)$ is only a third of what it was at $q=\pi/2$, but spread over a narrower range of frequencies (see Fig. 6). The bandwidth has shrunk to less than a third of the value it had at $q=\pi/2$. The relative $\psi\psi^*$ contribution to the intensity is even larger than at $q=\pi/2$, almost 100%. In this application, the method of analysis is stretched more closely to its limits because $q=\pi/4$ exists in fewer manageable system sizes. However, the data still make reliable line shape predictions possible.

The density of states $D_{zz}^{\psi\psi^*}(\pi/4,\omega)$, plotted in Fig. 9(a), rises discontinuously from zero to a finite value at the spectral threshold, $\Delta E\simeq 0.379J$. From there it increases gradually with gradually increasing slope and ends in a cusp singularity at the upper band edge.[25] The finite-N data for the scaled transition rates shown in Fig. 9(b) again suggest a smooth ω dependence in the form of a monotonically decreasing curve with enhanced steepness near both band edges. However, the countertrend of the density of states at

the upper band edge is of sufficient strength to produce a second maximum in the line shape again.

Also shown in Fig. 9 are the corresponding data for the $\psi\psi^*$ density of states, transition rates, and line shape at $q=3\pi/4$. Here the relative spectral weight carried by the $\psi\psi^*$ excitations is only 83% of the value at $q=\pi/2$, but that fraction is concentrated over a frequency band that has shrunk to 65% of the width at $q=\pi/2$, while the absolute intensity remains fairly high (87% of the value at $q=\pi/2$). Both quantities, which determine the $\psi\psi^*$ line shape, exhibit similar frequency dependences as we have already observed for the other two fixed-q scans. The density of states is divergent again at the upper boundary. The energy gap is now much larger, $\Delta E \simeq 0.899J$. The fact that the lower continuum boundary at $q=3\pi/4$ coincides with the upper continuum boundary at $q=\pi/4$ is a consequence of the quasiparticle dispersions as discussed previously.

VII. CONCLUSION

The spectrum of the completely integrable 1D $s=\frac{1}{2}$ Heisenberg antiferromagnet (1) can be generated in more than one way from multiple excitations of quasiparticles. The external magnetic field controls the nature of the ground state. In strong fields, it becomes the vacuum of magnons and in zero field the vacuum of spinons. The dynamically relevant collective excitations of specific quantum fluctuations in the two cases are then naturally described as composites of quasiparticles from the respective species and are likely to involve only a small number of quasiparticles.

In intermediate magnetic fields, neither the magnons nor the spinons provide a useful interpretation of dynamically relevant collective excitations for the same fluctuation operators. The ground state itself contains a macroscopic number of quasiparticles from one or the other of the two species. However, when it is reconfigured as the physical vacuum for psinons and antipsinons, then it turns out that the spin fluctuation operator S^z_q induces predominantly transitions to $\psi\psi^*$ states, which contain just one particle from each kind.

Similar to the magnon and the spinon, the psinon and the antipsinon are interacting quasiparticles in the Heisenberg model (1). In the $\psi\psi^*$ scattering states, the interaction energy of the psinon and the antipsinon is of order $O(N^{-1})$ whereas the interaction energy among magnons or spinons is of order $O(1)$. Hence, for $N\to\infty$, the $\psi\psi^*$ states join up in (q,ω) space to form a two-parameter continuum whose spectral boundaries and density of states are fully determined by the energy-momentum relations of the psinon and the antipsinon. Moreover, the scaled $\psi\psi^*$ transition rates converge for $N\to\infty$ toward a smooth function of q and ω.

We have exploited these asymptotic quasi-particle properties to extract line shape information for the dynamic structure factor $S_{zz}(q,\omega)$, which probes the spin fluctuations parallel to the applied magnetic field. The same quasiparticles will also play a dominant role in the spin fluctuations perpendicular to the field, but here different combinations of them make up the composition of the dynamically relevant collective excitations. In the dynamic spin structure factor $S_{-+}(q,\omega)$, for example, the spectral weight is almost completely carried by two-psinon excitations.[18]

In all likelihood, the psinon quasiparticles will also be useful for the analysis of thermal spin fluctuations in this model system. The peculiar spectral weight distributions found in recent complete diagonalization studies[26,27] of $S_{zz}(q,\omega)$ at $h=0$ and $T>0$, for example, indicate the presence of stringent selection rules between collective states coupled by the spin fluctuation operator S^z_q. In zero field, psinon vacua are densely spread across the entire energy range of the model. Each psinon vacuum can be used as the reference state of a $2m$-psinon expansion (9). If there are general selection rules related to psinon quasiparticles among transition rates $|\langle\lambda'|S^z_q|\lambda\rangle|^2$ within a given class K_r of Bethe ansatz solutions, they will have a strong impact on the spectral weight distribution in $S_{zz}(q,\omega)$ at all temperatures.

A question of considerable interest concerns the fate of the psinon and antipsinon quasiparticles in the presence of an interchain coupling, which is an inevitable complication in all physical realizations of spin chains. Any such interaction, even if treated summarily as a (mean) staggered field, is all but certain to destroy the exact solvability of the model and is likely to produce energy gaps and magnetization plateaus. One promising method for studying the effect of a staggered field on the spectrum and the dynamics of the Heisenberg model employs a rigorous set of evolution differential equations for the excitation energies and transition matrix elements, for which exact results such as established here via Bethe ansatz play the role of initial conditions.[31,32]

ACKNOWLEDGMENTS

We thank Andreas Klümper, Klaus Fabricius, and Alexander Meyerovich for interesting and useful discussions. Financial support from the URI Research Office (for G.M.) and from the DFG Schwerpunkt Kollektive Quantenzustände in elektronischen 1D Ubergangsmetallverbindungen (for M.K.) is gratefully acknowledged.

[1] H. Bethe, Z. Phys. **71**, 205 (1931).

[2] L. D. Faddeev and L. A. Takhtajan, Phys. Lett. **85A**, 375 (1981).

[3] A rigorous mapping between the two interpretations of the energy spectrum exists in a separable Hilbert subspace of a macroscopic system (Ref. 2).

[4] In some collective excitations, the quasiparticles form bound states, and the interaction energy remains significant for $N\to\infty$ even if only few quasiparticles are present (bound magnons are discussed in Ref. 28).

[5] M. Karbach, G. Müller, A. H. Bougourzi, A. Fledderjohann, and K.-H. Mütter, Phys. Rev. B **55**, 12 510 (1997).

[6] J. Des Cloizeaux and J. J. Pearson, Phys. Rev. **128**, 2131 (1962).

[7] T. Yamada, Prog. Theor. Phys. **41**, 880 (1969).

[8] D. A. Tennant, R. A. Cowley, S. E. Nagler, and A. M. Tsvelik, Phys. Rev. B **52**, 13 368 (1995).

[9] D. C. Dender, P. R. Hammar, D. C. Reich, C. Broholm, and G. Aeppli, Phys. Rev. Lett. **79**, 1750 (1997).

[10] P. R. Hammar, M. B. Stone, D. H. Reich, C. Broholm, P. J.

Gibson, M. M. Turnbull, C. P. Landee, and M. Oshikawa, Phys. Rev. B **59**, 1008 (1999).
[11] M. Karbach, K. Hu, and G. Müller, cond-mat/0008018 (unpublished).
[12] C. N. Yang and C. P. Yang, Phys. Rev. **150**, 321 (1966).
[13] R. B. Griffiths, Phys. Rev. **133**, A768 (1964).
[14] J. C. Bonner and M. E. Fisher, Phys. Rev. **135**, A640 (1964).
[15] M. Karbach, K. Hu, and G. Müller, Comput. Phys. **12**, 565 (1998).
[16] In the Haldane-Shastry model, where the spinons are noninteracting quasiparticles, the need for introducing new quasiparticles is less urgent (see Ref. 29).
[17] G. Müller, H. Thomas, H. Beck, and J. C. Bonner, Phys. Rev. B **24**, 1429 (1981).
[18] M. Karbach and G. Müller (unpublished).
[19] This kind of factorization was also used in Ref. 5 for the calculation of the exact two-spinon part of $S_{zz}(q,\omega)$ at $M_z=0$ via algebraic analysis and in a Lanczos study of $S_{zz}(q,\omega)$ for the Heisenberg and Haldane-Shastry models (Ref. 30).
[20] Not included in Fig. 8(b) is the contribution to $D^{\psi\psi^*}(\pi/2,\omega_{v*})$ of the $\psi\psi^*$ states in the narrow strip of the continuum that is folded over, because no fold exists in systems with $N\leqslant 32$, for which we have transition rate data available.
[21] It incorporates only the transition rate data from states whose excitation energies fall between the $\psi\psi^*$ continuum boundaries. That excludes a few data points from Fig. 8(b) near the upper band edge because of the residual quasiparticle interaction.
[22] F. D. M. Haldane, Phys. Rev. Lett. **45**, 1358 (1980).
[23] N. M. Bogoliubov, A. G. Izergin, and N. Y. Reshetikhin, J. Phys. A **20**, 5361 (1987).
[24] A. Fledderjohann, C. Gerhardt, K.-H. Mütter, A. Schmitt, and M. Karbach, Phys. Rev. B **54**, 7168 (1996).
[25] At $q=\pi/4$ the $\psi\psi^*$ continuum is not folded at the upper boundary.
[26] K. Fabricius, U. Löw, and J. Stolze, Phys. Rev. B **55**, 5833 (1997).
[27] K. Fabricius and U. Löw, Phys. Rev. B **57**, 13 371 (1998).
[28] M. Karbach and G. Müller, Comput. Phys. **11**, 36 (1997).
[29] J. C. Talstra and F. D. M. Haldane, Phys. Rev. B **50**, 6889 (1994).
[30] K. Lefmann and C. Rischel, Phys. Rev. B **54**, 6340 (1996).
[31] A. Fledderjohann, M. Karbach, and K.-H. Mütter, Eur. Phys. J. B **5**, 487 (1998).
[32] A. Fledderjohann, M. Karbach, and K.-H. Mütter, Eur. Phys. J. B **7**, 225 (1999).